ADVANCED FUNCTIONAL MATERIALS
www.afm-journal.de

Thiophene–Benzothiadiazole Co-Oligomers: Synthesis, Optoelectronic Properties, Electrical Characterization, and Thin-Film Patterning

By *Manuela Melucci,* Laura Favaretto, Alberto Zanelli, Massimiliano Cavallini, Alessandro Bongini, Piera Maccagnani, Paolo Ostoja, Gwennaelle Derue, Roberto Lazzaroni,* and *Giovanna Barbarella*

Newly synthesized thiophene (T) and benzothiadiazole (B) co-oligomers of different size, alternation motifs, and alkyl substitution types are reported. Combined spectroscopic data, electrochemical analysis, and theoretical calculations show that the insertion of a single electron-deficient B unit into the aromatic backbone strongly affects the LUMO energy level. The insertion of additional B units has only a minor effect on the electronic properties. Cast films of oligomers with two alternated B rings (B–T–B inner core) display crystalline order. Bottom-contact FETs based on films cast on bare SiO_2 show hole-charge mobilities of 1×10^{-3}–5×10^{-3} $cm^2 V^{-1} s^{-1}$ and I_{on}/I_{off} ratios of 10^5–10^6. Solution-cast films of cyclohexyl-substituted compounds are amorphous and do not show FET behavior. However, the lack of order observed in these films can be overcome by nanorubbing and unconventional wet lithography, which allow for fine control of structural order in thin deposits.

1. Introduction

Development of organic semiconductors with good thermal and chemical stability, solution processibility, tailored morphology, and high charge-carrier mobility is essential for applications in organic electronics and, more generally, in nanoscience.[1]

In this regard, design strategies allowing for fine control of the HOMO–LUMO energy levels in organic materials are a crucial issue. Indeed, injection of holes and electrons and absorption/emission properties depend on frontier-orbital energies and corresponding energy gaps.[2] To this end, alternation of electron-rich and electron-deficient heterocycles in conjugated oligomers and co-polymers to narrow the bandgap and tune the HOMO–LUMO energy levels has drawn much attention. Other key factors in optimizing the optical and transport properties of organic materials in thin films are the morphological organization and the structural order at mesoscopic length scales.[3]

Benzothiadiazole (B) is an electron-deficient fused heterocycle that, coupled to electron-rich partners, affords small bandgap molecular and polymeric π-conjugated materials. Alternation of thiophene (T) and B rings has been widely exploited for applications in devices such as photovoltaic cells, light-emitting diodes, and field-effect transistors. In fact, high ordering capability in thin films and morphologies suitable for applications as active layers in devices have been demonstrated.[4]

Herein, we report the synthesis of well-defined model BT oligomers of different size and investigate the effect of the number of B units on their optoelectronic properties by means of cyclovoltammetry, theoretical calculations, and UV and photoluminescence (PL) spectroscopy. The hole-transport properties in the bottom-contact field-effect transistor (FET) configuration were evaluated using solution-cast films as active elements. Finally, the role of cyclohexyl substituents on both electronic properties and morphology was investigated and nanorubbing[5] and micro molding in capillaries (MIMIC)[6] techniques were successfully applied to achieve control over

[*] Dr. M. Melucci, L. Favaretto, Dr. A. Zanelli, Dr. G. Barbarella
Istituto per la Sintesi Organica e la Fotoreattività (ISOF)
Consiglio Nazionale Ricerche
via P. Gobetti, 101, 40129 Bologna (Italy)
E-mail: mmelucci@isof.cnr.it

Dr. M. Cavallini
Istituto per i Materiali Nanostrutturati (ISMN)
Consiglio Nazionale Ricerche
via P. Gobetti 101, 40129 Bologna (Italy)

Prof. A. Bongini
Università di Bologna
Dipartimento di Chimica "G. Ciamician"
via F. Selmi, 2, 40122 Bologna (Italy)

Dr. P. Maccagnani, Dr. P. Ostoja
Istituto per la Microelettronica e i Microsistemi (IMM)
Consiglio Nazionale Ricerche
via P. Gobetti 101, 40129 Bologna (Italy)

Dr. G. Derue, Prof. R. Lazzaroni
Service de Chimie des Matériaux Nouveaux
Université de Mons/Materia Nova
20, Place du Parc, B-7000 Mons (Belgium)

DOI: 10.1002/adfm.200901424

© 2010 WILEY-VCH Verlag GmbH & Co. KGaA, Weinheim

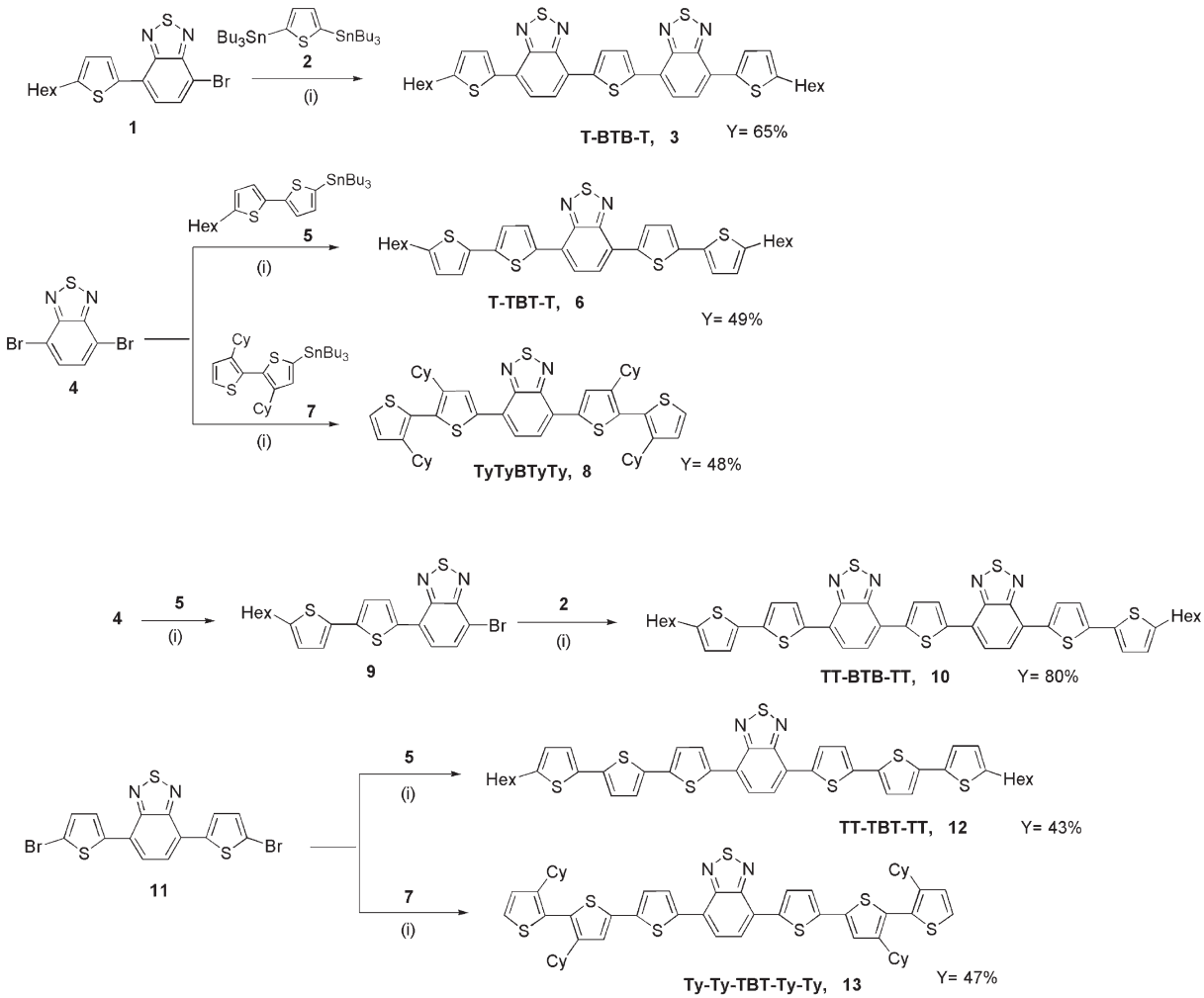

Scheme 1. Synthetic route to TB pentamers and heptamers. i) $Pd[AsPh_3]_4$, toluene, 112 °C. Hex = *n*-hexyl, Cy = cyclohexyl. Y = isolated yield.

molecular orientation and morphology in some of these compounds.

2. Results and Discussion

2.1. Synthesis

The synthetic route to T–B co-oligomers is outlined in Scheme 1. The Stille coupling reaction was employed to build up the oligomer backbone. Here, stannyl-derivatives **2**, **5**, and **7** were prepared under conventional metallation conditions (BuLi/ Bu_3SnCl, THF, −78 °C).

Then, pentamers **3**, **6**, and **8** and heptamers **10**, **12**, and **13** were synthesized by Pd(0)-mediated Stille coupling reaction in refluxing toluene, by using a catalytic amount (5 mol%) of in situ prepared $Pd[AsPh_3]_4$ as the catalyst. Satisfactory yields were achieved in all cases upon purification by chromatography and further crystallization steps. On increasing the number of B units, a strong decrease in solubility in common organic solvents was observed. Compounds **8** and **13**, having bulky substituents in the beta position of the external thiophene rings, displayed much greater solubility than their analogues with terminal alkyl chains.

2.2. Optical Properties and Cyclovoltammetry Data

UV–vis absorption and emission spectra of pentamers **3** and **6** and heptamers **10** and **12** are shown in Figure 1a, and the maximum absorption and emission wavelengths of all compounds are summarized in Table 1. TTBTT (**6**) and TTTBTTT (**3**) show the first maximum at 360 nm and 380 nm, respectively, and at 327 nm and 358 nm for TBTBT and TTBTBTT, respectively. The second band is located in the region 510–540 nm for all compounds. The spectra show a redshift of the maximum absorption and emission wavelength on going from pentamers to heptamers, independently of the type of B–T alternation motif.

Cyclohexyl-substituted oligomers show a blueshift when compared to hexyl-terminated analogues (Table 1). This can be

© 2010 WILEY-VCH Verlag GmbH & Co. KGaA, Weinheim

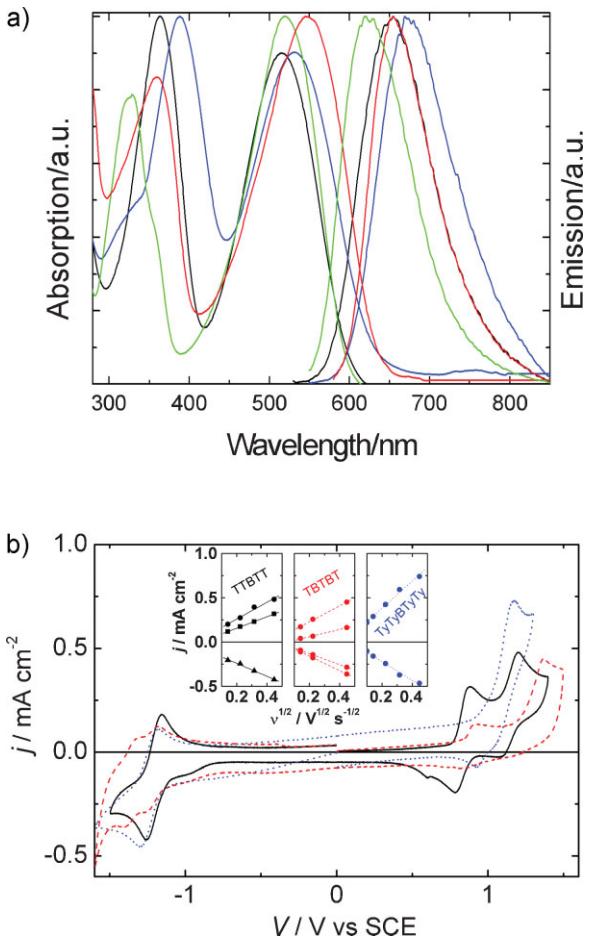

Figure 1. a) Normalized absorption and emission spectra of compounds **3**, **6**, **10**, and **12** (green, black, red, and blue lines, respectively) in CH_2Cl_2. b) CVs on Pt electrode in CH_2Cl_2 0.1 mol L^{-1} $(C_4H_9)_4NClO_4$ at 0.2 V s^{-1} and room temperature of TTBTT (**6**, ——), TBTBT (**3**,- - -) and TyTyBTyTy (**8**, ····) 1.5 mmol · L^{-1}. Inset: peak current versus the square root of the scan rate.

ascribed to the distortion effects of the bulky cyclohexyl groups, which reduce the molecule overall planarity and the π-electron conjugation. However, the Stokes shift values are comparable to those of hexyl-terminated systems, indicating that cyclohexyl substituents do not prevent planarization in the excited state.

When comparing co-oligomers of the same size, only slight differences can be found in the absorption features (e.g. TTBTT vs. TBTBT or TTTBTTT vs. TTBTBTT). Moreover, in all cases, insertion of B units results in a marked red shift of λ_{max} with respect to unsubstituted all-thiophene oligomers, as shown, for example, by comparison of quinquethiophene TTTTT ($\lambda_{max} = 416$ nm)[7] and co-oligomer TTBTT ($\lambda_{max} = 510$ nm).

This indicates that BT-based systems are characterized by higher π-conjugation extent, in agreement with the greater molecular rigidity and π-polarization already observed for donor–acceptor–donor TBT-based systems.[8] Interestingly, the observed redshift is higher than that promoted by insertion of a central thienyl-S,S-dioxide electron deficient moiety (O) in the backbone of unsubstituted oligothiophenes (TTOTT, $\lambda_{max} = 469$ nm).[9] It is noteworthy that thienyl-S,S-dioxide insertion is among the most effective strategies to affect the HOMO–LUMO energy levels of oligothiophenes.[10] Table 1 also shows that on increasing the co-oligomer size, a further redshift is observed, in agreement with the trend observed for conventional oligothiophenes.[11] Here, the longer compounds TTTBTTT (**12**) and TTBTBTT (**10**) show a red shift of λ_{max} in the order of 80–90 nm with respect to heptathiophene TTTTTTT ($\lambda_{max} = 450$ nm).[12] Again, when compared to the insertion of thienyl-S,S-dioxide in heptathiophene (TTTOTTT, $\lambda_{max} = 505$ nm),[13] the B system appears much more effective in terms of redshifting λ_{max}. On going to photoluminescence spectra, **12** shows a greater Stokes shift than **10** (139 vs. 116 nm) suggesting a higher degree of planarity in the excited state for T–B–T compared to B–T–B inner core based oligomers.

Cyclic voltammograms (CVs) of pentamers TTBTT, TBTBT, and TyTyBTyTy are shown in Figure 1b. The CV of TTBTT (**6**, solid line in Fig. 1b) shows one reduction and two oxidation quasi-reversible waves. The reduction and oxidation peak potentials are located at −1.26 V, 0.88 V, and 1.21 V, respectively. TBTBT (**3**, red line in Fig. 1b) shows a first quasi-reversible oxidation wave with the maximum at a potential just 0.03 V more positive than that for the corresponding oxidation of **6**, but the second oxidation wave appears irreversible with the maximum about 0.17 V more positive than that of **6**. On the other hand, TyTyBTyTy (**8**, blue line in Fig. 1b) shows only one oxidation wave with the peak potential 0.29–0.26 V more positive than that of **6** and **3**, as expected, because of the distortion effect of the bulky cyclohexyl groups which decreases the overall conjugation extent.

In the cathodic region, the presence of two B groups induces the rising of a second reversible reduction wave with the peak potential

Table 1. Absorption and emission wavelengths and CV data of compounds **3**, **6**, **8**, **10**, **12**, and **13**.

Compound	λ_{max} [nm] [a]	λ_{PL} [nm]	E_g [eV] [b]	E^0_{ox1} [V] [c]	E^0_{ox2} [V] [c]	E^0red [V] [c]	*i.p.* [eV] [d]	*e.a.* [eV] [d]
TBTBT, **3**	520	624	2.08	0.86	1.37	−1.21 [f]	−5.54	−3.47
TTBTT, **6**	510	656	2.07	0.83	1.16	−1.21	−5.51	−3.47
TTBTBTT, **10**	540	656	1.96	0.68	1.06 [e]	−1.13	−5.36	−3.55
TTTBTTT, **12**	533	672	1.95	0.77	1.00 [e]	−1.16	−5.45	−3.52
TyTyBTyTy, **8**	480	621	2.21	1.04	– [g]	−1.24	−5.72	−3.44
TyTyTBTTyTy, **13**	519	657	2.03	0.93	1.10	−1.18	−5.61	−3.50

[a] In CH_2Cl_2. [b] Energy-gap evaluated as $E_g = 1240\ \lambda^{-1}_{onset}$. [c] E^0 is the average value between the peak potential and the related reverse one referred to SCE. [d] $i.p. = e(4.68 + E^0ox1)$ and $e.a. = e(4.68 + E^0red)$ [15]. [e] peak potential, the process is irreversible, [f] TBTBT shows a second quasi-reversible reduction wave at −1.35 V. [g] Non-detectable.

© 2010 WILEY-VCH Verlag GmbH & Co. KGaA, Weinheim

0.15 V more negative than the first one, suggesting that the radical anions are localized on the B groups that interact only because of electrostatic repulsion. In contrast with oxidation, the reduction wave of TyTyBTyTy, **8** (−1.29 V) approaches the potentials of both TTBTT (**6**) and TBTBT (**3**), confirming that the outer thiophene rings do not affect the energy of the LUMO orbital, which is mostly localized on the B units (see theoretical calculations in Fig. 2a).

The insets of Figure 1b show the peak current density versus the square root of the scan rate. All the peaks corresponding to first oxidation and reduction fit to straight lines, showing that the redox processes are driven by the diffusion in solution. The trends for the second oxidation peaks are similar but the correlation is not as good. The slopes of those straight lines are comparable, except that of TyTyBTyTy (**8**) oxidation which is higher, even with respect to that of the reduction. This suggests the contribution of two simultaneous monoelectronic oxidations, rather than a higher diffusion coefficient that mismatches the bigger hindrance of TyTyBTyTy. CVs of heptamers **10**, **12**, and **13** showed the same trend observed for the corresponding pentamers and are reported in the Supporting Information (Fig. S8). Data in Table 1 shows that the reduction potentials of TTBTBTT (**10**) and TTTBTTT (**12**) are 0.08–0.05 V less negative than those of TBTBT (**3**) and TTBTT (**6**), in agreement with the increase of the chain length. On the other hand, the two oxidation waves appear irreversible[14] and partially overlapped. The oxidation potentials result less positive than those of the shorter co-oligomers with a decrease related to the inverse number of adjacent thiophenes. Indeed, the decrease from single thiophene terminal to bithiophene is 0.08 V but that from bithiophene to terthiophene is only 0.03 V. The steric hindrance of the cyclohexane group undoes this shift in TyTyTBTTyTy, **13**.

In summary, the CV values in Table 1 show that the insertion of a B ring leads to a marked increase in electron affinity with respect to a conventional oligothiophene of the same size. For instance, replacing a T ring with a B ring in a end-capped quinquethiophene taken as reference system (TTTTT)[16] shifts the reduction about 0.9 V toward less negative potentials ($E_{red} = -2.13$ V for TTTTT vs. −1.21 for **3** and **6**).[16] However, the first oxidation shifts only of about 0.05 V toward less positive potentials, reduce the overall energy gap of TTBTT (**6**) of 0.9 eV with respect to the model TTTTT ($E_{ox} = 0.92$ V[16]). Finally, comparison of B with the electron-deficient thienyl-S,S-dioxide unit (O), which shifts the reduction of TTOTT[9] of about 1V with respect to TTTTT,[16] indicates that B is less efficient than O in increasing the electron affinity of thiophene oligomers. However, contrary to thienyl-S,S-dioxide, B does not increase the oxidation potential, leading to a comparable electrochemical energy gap for pentamers TTBTT and TTOTT[9] (2.14 vs. 2.21 eV). To gain some insight into the electronic properties of BT based co-oligomers, the electronic densities of the frontier molecular orbitals and their energy values were determined by semiempirical calculations. Trimers BTB and TBT and all-thiophene oligomers of comparable size were also considered as reference compounds. Figure 2 is representative of all compounds and compares the electron densities of pentamers TTBTT (**6**) and TBTBT (**3**) with those of TTTTT (electron densities of heptamers are reported in Fig. S9 of the Supporting Information). In the figure, the calculated HOMO and LUMO energy values are also reported. It can be seen that in all cases the HOMO orbitals are homogeneously distributed all over the molecule. In contrast, the LUMO orbitals in BT co-oligomers show a higher density on the benzothiadiazole group(s), in agreement with what has been observed upon the insertion of thienyl-S,S-dioxide units.[10,13,17] The calculations also show that the insertion of a single B unit has only a minor effect on the HOMO energy level of thiophene oligomers, while it strongly shifts the LUMO energy levels toward less negative values, that is, closer to that of the benzothiadiazole ring (−1.66 eV). Increasing the length of the oligomer backbone by adding one or two terminal thiophene rings to trimers TBT and BTB (Fig. 2b) leads to substantial changes in the HOMO energy but only minor changes in the LUMO energy, consistent with the localization of the LUMO orbital on the B units. In agreement with electrochemical data, the insertion of a second B unit leads to a further stabilization of the LUMO, by about −0.14 eV. This effect is as strong as that of the addition of an extra T unit on the HOMO energy (e.g., TTBTT HOMO = −6.54 eV; TTTBTTT HOMO = −6.40 eV).

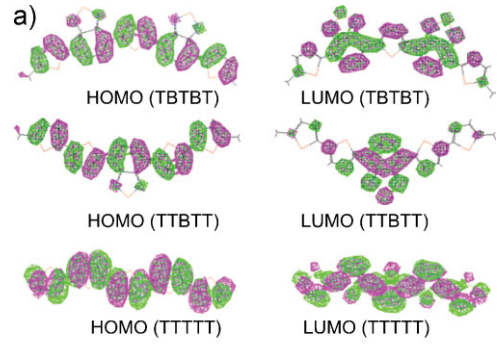

b)

Item	HOMO [eV]	LUMO [eV]
TBT	-7.13	-1.79
BTB	-7.31	-1.94
TTT	-6.93	-0.54
TTBTT	-6.54	-1.77
TBTBT	-6.72	-1.91
TTTTT	-6.61	-0.77
TTTBTTT	-6.40	-1.81
TTBTBTT	-6.55	-1.95
TTTTTTT	-6.49	-0.87

Figure 2. a) Calculated electronic densities of the frontier molecular orbitals of pentamers TTBTT, TBTBT and quinquethiophene TTTTT. b) HOMO–LUMO energy values calculated by semiempirical calculations for all compounds. Values for thiophene oligomers of comparable size are given for comparison.

2.3. Thin-Film Morphology, Electrical Characterization, and Patterning

Thin films of all compounds were prepared by drop casting 20 μL of a 1 g L^{-1} ($CHCl_3$ or toluene) solution on glass. The samples were investigated by atomic-force microscopy (AFM) in intermittent

© 2010 WILEY-VCH Verlag GmbH & Co. KGaA, Weinheim

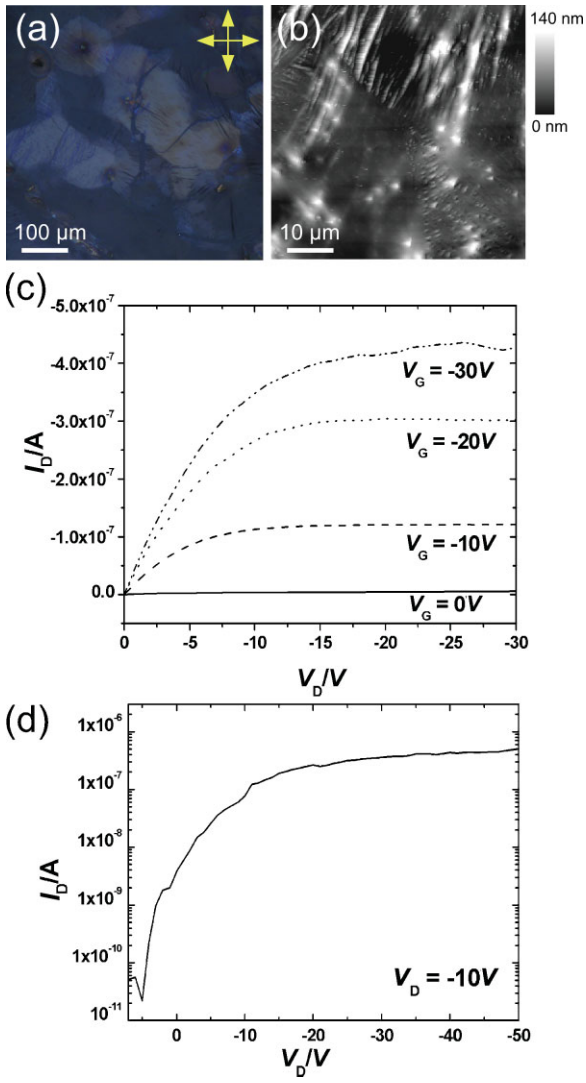

Figure 3. Morphology and electrical performance in FET configuration of cast film (from toluene) on bare SiO_2 of compound **10**. a) Optical microscopy image with cross polarizers showing a polycrystalline film and b) corresponding AFM image. c) Current–voltage plot for a bottom-contact FET device at $V_G = 0$ V, -10 V, -20 V, -30 V, $V_T = -5$ V. d) Semi-logarithmic plot of I_D versus V_{GS} at $V_{DS} = -10$ V.

contact mode and by optical microscopy. Thin films of hexyl-terminated oligomers showed birefringent structures (Fig. 3a) independent of the number of B units and co-oligomer size. Observation with crossed polar optical microscopy showed the typical optically anisotropic material behavior: the background did not transmit light, while the crystals appeared coloured under crossed polars, with colours ranging from violet to yellow depending on local thickness. By rotating the crystal orientation to the polarised light, the crystals extinguish only in some portions of the structure. This behavior suggests that each structure is formed by several domains with different orientation. Hole-charge-transport capabilities were investigated for such crystalline materials in a bottom contact–FET configuration. The devices realized by using drop-cast film on bare SiO_2 (2 mg mL^{-1}, toluene, room temperature) of compounds **3** (TBTBT) and **10** (TTBTBTT)

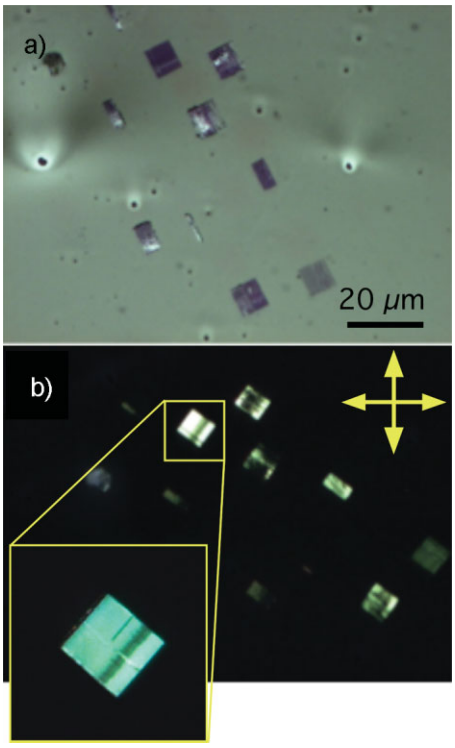

Figure 4. Optical micrographs of nanorubbed thin film of **13** deposited on glass. a) Image in bright field and b) corresponding image between crossed polars. The crossed polars are oriented as shown by the arrows. The inset shows a detail of about $10 \times 10\,\mu m^2$ rubbed zone.

showed charge mobility of $\mu_{FETh} = 5 \times 10^{-3}\,cm^2\ V^{-1}s^{-1}$ and $1 \times 10^{-3}\,cm^2\,V^{-1}s^{-1}$, calculated from the saturation regime, and high I_{on}/I_{off} ratios of 10^6 and 10^5, respectively. A current–voltage plot and a semilogarithmic plot I_D versus V_{GS} for compound **10** are shown in Figure 4c and d while the corresponding curves for compound **3** are reported in the Supporting Information (Fig. S10).

The electrical properties of compounds **6** (TTBTT)[4b,c] and **12** (TTTBTTT)[4b] with only one B unit, evaluated under the same experimental conditions, have already been reported. Interestingly, pentamer **6** (TTBTT), showed charge mobility $\mu_{FETh} = 4 \times 10^{-4}\,cm^2\ V^{-1}s^{-1}$ ($I_{on}/I_{off} = 10^3$), while no FET behaviour was observed for drop-cast films of heptamer **12**. These results indicate that increased B-unit number could substantially improve the hole transport in BT co-oligomers. It is likely that the enhanced rigidity[4a,8] and dipole-induced intermolecular stacking[4f] promoted by the acceptor–donor–acceptor alternated motif favour intermolecular overlap and improve the charge-transport capabilities in oligomers containing the B–T–B motif.

It is worth noting that enhanced performances can be expected for our B/T co-oligomers upon tailored-device optimization. Indeed, higher mobility values on self-assembled monolayer (SAM)-modified SiO_2 substrate in top contact FETs have been reported for compound **6**.[4c]

In contrast to the previously described BT co-oligomers, no FET behaviour was found for cyclohexyl-substituted **8** and **13** under our experimental conditions. For these compounds, amorphous films

© 2010 WILEY-VCH Verlag GmbH & Co. KGaA, Weinheim

with no particular optical signature were observed, this being likely due to the bulky cyclohexyl groups, which could prevent self-organization. However, local ordering in those amorphous films was successfully promoted by nanorubbing. Nanorubbing consists of applying a unidirectional constraint on a surface with the tip of an AFM operated in contact mode. The high precision of the positioning of the tip and the force exerted makes it a powerful tool for controlled surface modification on the micro- or nanoscale. Nanorubbing has been recently used to locally align liquid crystals[5c] and conjugated polymers.[5a,b,d] In thin films of cyclohexyl-substituted compounds **8** and **13**, the optical properties of the rubbed zones are clearly different, while the AFM images do not reveal any significant morphological modification.

As shown in Figure 4, rubbed zones exhibit a clear contrast in bright-field optical microscopy and appear colored when observed with crossed polars. These zones show the typical behavior of optical anisotropic materials: a complete extinction of the nanorubbed areas is observed when the polarization direction is either parallel or perpendicular to the rubbing direction, while the highest brightness is observed when the polarization directions are rotated 45° to the rubbing directions. This behavior suggests that the surface orientation induced initially by nanorubbing at the surface (in polymers, rubbing typically induces alignment over a depth of 10–20 nm) propagates through the entire thickness of the film. This result is particularly relevant because it can be obtained only by rubbing; in fact the simple application of pressure (for example by imprinting)[18] does not induce any relevant effect in the optical properties of **8** and **13** thin films.

Unconventional lithography was also successfully employed for the patterning of compound **8**. In particular, we used MIMIC to obtain a micrometric pattern of **8** (therefore optically accessible) with controlled size and position. In MIMIC, a polydimethylsiloxane mold is placed on to a flat surface to effectively form microchannels (Fig. 5a1).[6,19]

When the solution is poured at the open end of the stamp, the liquid fills the microchannels by capillary action (Fig. 5a2). After the complete evaporation of the solvent (24 hours in air at room temperature) the stamp is removed and the sample characterized by AFM and optical microscopy. AFM studies of the structures of **8**, printed by MIMIC on glass, reveal the formation of micrometric stripes of ~2-μm width, coherent with the size of the stamp. Optical images obtained by polarized microscopy (Fig. 5b) show the typical behavior of optically anisotropic materials exhibiting birefringence. In particular, the μ-stripes appear homogeneously colored; this indicates that their thickness is almost constant over the entire stripe. The μ-stripes extinguish in four positions at intervals of 90°. Thus, we can deduce that the confined deposition by MIMIC has induced a coherent, long-range order along the direction of the stripes.

Nanorubbing and MIMIC experiments on the highly soluble cyclohexyl substituted co-oligomers **8** and **13** show that, despite the intrinsic tendency to give amorphous cast films, good local ordering at micrometer scale can be achieved by means of appropriate patterning techniques.

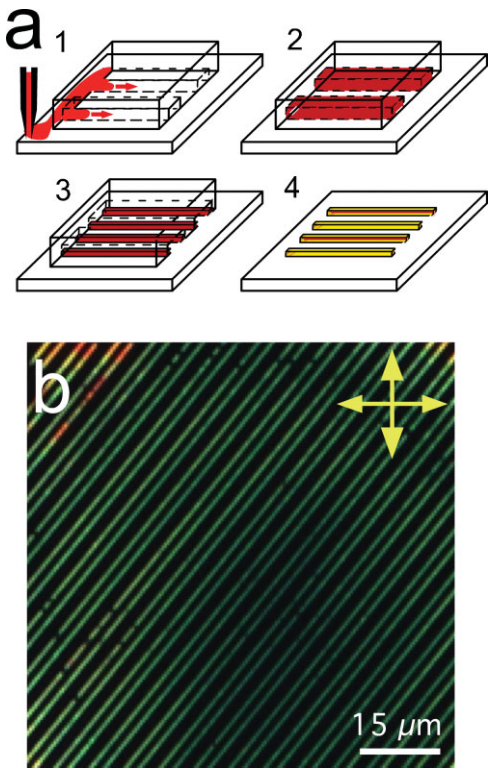

Figure 5. a) Scheme of MIMIC method [19]. b) Optical micrograph of micrometric stripes of **8** fabricated by MIMIC on glass taken with crossed polars oriented along the axes of the image.

3. Conclusions

In summary, our data show that insertion of a benzothiadiazole unit (B) as inner unit in the oligothiophene backbone has a marked effect on the LUMO energy level of the resulting co-oligomer. Addition of further electron-accepting B units spaced by thienyl rings has a negligible effect on both electron affinity and morphology. Polycrystalline cast films were observed for hexyl-terminated co-oligomers, independently of the molecular structure and number of B units. However, initial electrical measurements showed improved electrical performances for both pentamers and heptamers with two B inner units. The insertion of bulky β-cyclohexyl substitution greatly increases the solubility of the longer oligomers but affects the overall degree of planarity, hence the extent of π-conjugation. As a result, blueshifts of the maximum absorption and emission in cast films are observed compared to terminal-substituted co-oligomers. Solution-cast films of cyclohexyl-substituted compounds are amorphous. However, the lack of order in thin films of these compounds can be overcome by nanorubbing and MIMIC techniques, to obtain ordered structures. We believe that the results presented herein will be useful to the design of BT-based materials with tailored electronic properties and enhanced charge-transport capabilities. Detailed electrical characterization (p–n type) of all compounds is currently under way.

4. Experimental

Synthesis: Bis-4,7-(5′-hexyl-2,2′-bithien-5yl)-2,1,3-benzothiadiazole TTBTT, **6**, and bis-4,7-(5″-hexyl-2:2′, 5′:2″-terthien-5yl)-2,1,3-benzothiadiazole TTTBTTT, **12**, were synthesized as described elsewhere [4b,c].

© 2010 WILEY-VCH Verlag GmbH & Co. KGaA, Weinheim

General Procedure for Stille Cross Coupling: $Pd[AsPh_3]_4$, generated in situ, was prepared by a refluxing solution of triphenylarsine $AsPh_3$ and tris(benzylidene acetone) dipalladium(0)chloroform adduct Pd_2dba_3 (5 mol% of Pd) in dry toluene under nitrogen. Then a toluene solution of bromo/dibromoderivative (1 equiv.) was added at reflux temperature and finally the proper stannyl derivative (1.1/2.2 equiv.) added dropwise. After 6 hours, the solution was cooled to room temperature and the crude product was chromatographed on silica gel or alumina. Finally, crystallization from toluene afforded the target compounds. In the case of compound **1**, the reaction was carried out under microwave assistance.

4-(5-Hexyl-thien-2-yl)-7-bromo-2,1,3-benzothiadiazole, ***1***: A microwave-oven reactor was charged with Pd_2dba_3 (16 mg, 15 μmol), $AsPh_3$ (37 mg, 0.12 mmol), and 16 mL of toluene, and the mixture was irradiated until it turned black. Then, dibromo-2,1,3-benzothiadiazole (0.147 g, 0.0005 mol) in 4 mL of toluene was introduced and the mixture was irradiated for 1 minute at 90 °C. Finally, 2-hexyl-5-tributhylstannylthiophene in 5 mL of toluene was added dropwise and the resulting mixture was irradiated for an additional 1 h. The solvent was evaporated and the crude chromatographed on Al_2O_3 using a solution of Et_2O (5%) and petroleum ether (95%) → Et_2O. Compound **1** was obtained as an orange powder in 60% yield (0.11 g).

m.p. 45 °C; ^{1}H NMR (400 MHz, $CDCl_3$ TMS): $\delta = 7.91$ (d, $J = 3.6$ Hz, 1H), 7.80 (d, $J = 7.6$Hz, 1H), 7.61 (d, $J = 7.6$ Hz, 1H), 6.86 (d, 1H, $J = 3.6$ Hz), 2.87 (m, 2H), 1.74 (m, 2H), 1.34 (m, 6H), 0.90 (m, 3H). ^{13}C NMR (100 MHz, $CDCl_3$, TMS): $\delta = 153.8$, 151.8, 148.6, 135.9, 132.3, 128.1, 127.5, 125.4, 125.1, 111.5, 31.6, 30.3, 29.7, 28.8, 22.6, 14.1; λ_{max} (CH_2Cl_2) = 424 nm; MS (70 eV, EI): m/z 380-382 ($M^{\cdot+}$).

Bis-2,5-[4-(5′-hexyl-thieno) 2,1,3-benzothiadiazole-7yl]-thiophene, TBTBT, ***3***: Deep purple powder in 65% of yield. m.p. 182 °C; ^{1}H NMR (400 MHz, $CDCl_3 + CS_2$, TMS): $\delta = 8.21$ (s, 2H), 7.97 (d, $J = 4$Hz, 2H), 7.93 (d, $J = 7.6$ Hz, 2H), 7.80 (d, $J = 7.6$ Hz, 2H), 6.86 (d, $J = 4$ Hz, 2H), 2.90 (m, 4H), 1.76 (m, 4H), 1.38 (m, 12H), 0.93 (m, 6H). ^{13}C NMR (100 MHz, $CDCl_3 + CS_2$, TMS): $\delta = 152.5$, 147.9, 146.7, 140.3, 136.7, 128.3, 127.8, 126.4, 125.6, 125.3, 125.0, 124.8, 31.7, 31.6, 30.4, 28.9, 22.7, 14.2; λ_{max} (CH_2Cl_2) = 520 nm; MS (70 eV, EI): m/z 683 ($M^{\cdot+}$); Anal. calcd for $C_{36}H_{36}N_4S_5$: C, 63.12; H, 5.30. Found: C, 63.21; H, 5.39.

Bis-4,7-(3,3′-dicyclohexyl-2,2′-bithien-5yl)-2,1,3-benzothiadiazole, TyTyBTyTy, ***8***: Chromatography performed on standard alumina using pentane→3% Et_2O, followed by crystallization from toluene, afforded compound **8** as a red powder (48% yield). M.p. > 200°; ^{1}H NMR (400 MHz, $CDCl_3$, TMS): $\delta = 8.13$ ppm (s, 2 H), 7.85 ppm (s, 2H), 7.35 (d, $J = 5.6$ Hz, 2H), 7.05 (d, $J = 5.2$ Hz, 2H), 2.64 (m, 4H), 1.50 (m, 40H). ^{13}C NMR (100 MHz, $CDCl_3$, TMS: $\delta = 152.6$, 149.0, 148.0, 139.2, 129.5, 127.3, 127.3, 126.5, 126.0, 125.7, 125.4, 38.3, 38.2, 34.5, 34.4, 26.6, 26.5, 26.0; λ_{max} (CH_2Cl_2) = 480 nm. MS (70 eV, EI): m/z 791 ($M^{\cdot\ -1}$). Anal. calcd for $C_{46}H_{52}N_2S_5$: C, 69.65; H, 6.61. Found: C, 69.57; H, 6.53.

4-(5′-hexyl-2,2′-bithien-5yl)-7-(bromo)-2,1,3-benzothiadiazole, ***9***: deep orange powder, 40% yield, m.p. 101 °C; ^{1}H NMR (400 MHz, $CDCl_3$, TMS): $\delta = 8.00$ (d, $J = 4$Hz, 1H), 7.82 (d, $J = 7.6$Hz, 1H), 7.66 (d, $J = 7.6$ Hz, 1H), 7.16 (d, $J = 4$ Hz, 1H), 7.09 (d, J = 3.2Hz, 1H), 6.72 (d, $J = 3.2$ Hz, 1H), 2.81 (m, 2H), 1.70 (m, 2H), 1.34 (m, 6H), 0.90 (m, 3H). ^{13}C NMR (100 MHz, $CDCl_3 + CS_2$, TMS): $\delta = 151.6$, 150.1, 146.3, 139.9, 136.4, 134.3, 132.3, 128.8, 126.9,125.1, 125.0, 124.0, 123.8, 111.9, 31.6, 30.2, 29.7, 28.8, 22.6, 14.1; λ_{max} (CH_2Cl_2) = 459 nm; MS (70 eV, EI): m/z 462-464 ($M^{\cdot+}$).

Bis-2,5-[4-(5″-hexyl-2,2′-bithien-5′yl)-2,1,3-benzothiadiazole-7yl]-thiophene, TTBTBTT, ***10***: Black solid, 80% yield. m.p. 230 °C; ^{1}H NMR (400 MHz, $CDCl_3 + CS_2$, TMS): $\delta = 8.25$ (s, 2H), 8.07 (d, $J = 4.0$ Hz, 2H), 7.96 (d, $J = 7.6$Hz, 2H), 7.85 (d, $J = 7.6$ Hz, 2H), 7.15 (d, $J = 4.0$ Hz, 2H), 7.07 (d, $J = 3.6$ Hz, 2H), 6.70 (d, $J = 3.6$ Hz, 2H) 2.83 (m, 4H), 1.73 (m, 4H), 1.38 (m, 12H), 0.93 (m, 6H); λ_{max} (CH_2Cl_2) = 540 nm; MS (70 eV, EI): m/z 848 ($M^{\cdot+}$). Anal. calcd for $C_{44}H_{40}N_4S_7$: C, 62.23; H, 4.75. Found: C, 62.32; H, 4.86.

Bis-4,7-(3′,3″-dicyclohexyl-2:2′,5′:2″-terthien-5yl)-2,1,3-benzothiadiazole TyTyTBTTyTy, ***13***: The crude was purified by chromatography (silica gel, pentane: CH_2Cl_2 5% → pentane CH_2Cl_2 20%) followed by crystallization from n-heptane (47% yield).

Purple solid, m.p. 142 °C ^{1}H NMR (400 MHz, $CDCl_3$, TMS): $\delta = 8.03$ (d, $J = 3.6$ Hz, 2 H), 7.87 (s, 2H), 7.33 (d, $J = 5.2$ Hz, 2 H), 7.24 (d + s, 4H), 7.04 (d, $J = 5.6$ Hz, 2 H,), 2.60 (m, 4H), 1.50 (m, 40H). ^{13}C NMR (100 MHz, $CDCl_3$, TMS): $\delta = 152.5$, 148.9, 148.1, 139.1, 137.8, 137.0, 128.2, 127.4, 127.1, 126.5, 125.9, 125.5, 125.1, 124.3, 123.6, 38.3, 38.2, 34.4, 34.3, 26.6, 26.0.; λ_{max} (CH_2Cl_2) = 519 nm; MS (70 eV, EI): m/z 956 ($M^{\cdot+}$). Anal. calcd for $C_{54}H_{56}N_2S_7$: C, 67.74; H, 5.90. Found: C, 67.82; H, 6.01.

Ultraviolet and visible (UV–vis) absorption and emission spectra were recorded by using a Perkin–Elmer Lambda 20 and a Perkin–Elmer LS 50 B spectrometer, respectively (CH_2Cl_2 solution, conc. about 10^{-5} M).

Redox potentials were determined at room temperature in CH_2Cl_2 (Merck, Uvasol, distilled over P_2O_5 and stored under Ar pressure) with 0.1 mol L^{-1} $(C_4H_9)_4NClO_4$ (Fluka, puriss. crystallized from CH_3OH and vacuum dried). Cyclic voltammetry (CV) was performed at several scan rates in the range 0.02–0.2 V s^{-1} after Ar bubbling in a three compartment glass electrochemical cell under Ar pressure, by using an AMEL electrochemical system model 5000. Working electrode was semi-spherical Pt (area 0.05 cm^2), reference electrode was saturated calomel electrode (SCE) and auxiliary electrode was a Pt wire. The potential of SCE with the liquid junction to CH_2Cl_2 0.1mol L^{-1} $(C_4H_9)_4NClO_4$ resulted −0.475 V versus ferrocene/ferricinium redox couple [20].

Calculations were carried out by HyperChem integrated package [21]. Frontier orbitals were calculated by ZINDO/S calculations on PM3 optimized geometry for the metyl end-capped molecules taken as simplified models.

The nanorubbing process was performed with a Nanoscope IIIa AFM microscope working in contact mode. The tips are made of antimony-doped silicon with a spring constant of 2 ± 0.5 N/m [22]. Typically 10 consecutive rubbing scans were carried out with the AFM tip in order to induce a sufficient deformation on the deposits. The loading force applied by the tip on the film during nanorubbing is approximately 200 nN, as calculated from the approach–retract curves.

A Nikon Eclipse 80i optical microscope was used for optical measurements. The images were recorded with a digital color camera Nikon Coolpix 5400. Glass substrate were furnished by Knittel gläser and were washed with Acetone spectroscopic grade (Aldrich) before use.

For FET fabrication, heavily doped ⟨100⟩ n–Si wafers were used as substrates, and 150-nm thick layer of SiO_2 (grown by thermal oxidation) was used as the gate dielectric. Au (80 nm) was evaporated and photolithographically defined to obtain the electrodes for gate, source and drain. The source–drain electrodes have a circular structure, with a channel width of 1880 μm and a channel length of 40 μm. Thin films were prepared by casting deposited on top of the substrates. The electrical measurements were performed using a computer controlled parametric characterization system at room temperature under atmospheric pressure conditions.

Acknowledgements

This work was partially supported by projects FIRB RBNE03S7XZ_005 (SYNERGY), PRRIITT-Misura 4.A PROMINER and (MC) ESF-EURYI DYMOT. Research in Mons was supported by the Science Policy Office of the Belgian Federal Government (PAI 6/27) and FNRS-FRFC. Supporting Information is available online from Wiley InterScience or from the author.

Received: June 30, 2009
Published online: January 7, 2010

[1] a) S. Liu, W. M. Wang, A. L. Briseno, S. C. B. Mannsfeld, Z. Bao, *Adv. Mater.* **2009**, *21*, 16. b) S. Allard, M. Forster, B. Souharce, H. Thiem, U. Scherf, *Angew. Chem. Int. Ed.* **2008**, *47*, 2. c) A. R. Murphy, J. M. J. Fréchet, *Chem. Rev.* **2007**, *107*, 1066. d) J. Zaumseil, H. Sirringhaus, *Chem. Rev.* **2007**, *107*, 1296. e) C. Reese, Z. Bao, *Mater. Today* **2007**, *10*, 20. f) A. Facchetti, *Mater. Today* **2007**, *10*, 28. g) M. Cavallini, P. Stoliar, J. F. Moulin, M. Surin, P. Leclère, R. Lazzaroni, D. W. Breiby, J. W. Andreasen, M. M. Nielsen, P. Sonar, A. C. Grimsdale, K. Müllen, F. Biscarini, *Nano Lett.* **2005**, *5*, 2422.

© 2010 WILEY-VCH Verlag GmbH & Co. KGaA, Weinheim

[2] a) A. Mishra, C.-Q. Ma, P. Bäuerle, *Chem. Rev.* **2009**, *109*, 1141. b) G. Barbarella, M. Melucci, G. Sotgiu, *Adv. Mater.* **2005**, *17*, 1581. c) J. Roncali, *Chem. Rev.* **1997**, *97*, 173.
[3] a) J. M. Mativetsky, M. Kastler, R. C. Savage, D. Gentilini, M. Palma, W. Pisula, K. Müllen, P. Samorì, *Adv. Funct. Mater.* **2009**, *19*, 2486. b) M. Mas-Torrent, C. Rovira, *Chem. Soc. Rev.* **2008**, *37*, 827. c) B. A. Jones, A. Facchetti, M. R. Wasielewski, T. J. Marks, *Adv. Funct. Mater.* **2008**, *18*, 1329. d) V. Coropceanu, J. Cornil, D. A. da Silva, Y. Olivier, R. Silbey, J. L. Brédas, *Chem. Rev.* **2007**, *107*, 926. e) H. Sirringhaus, *Adv. Mater.* **2005**, *17*, 2411. f) P. Leclère, M. Surin, O. Henze, P. Jonkheijm, F. Biscarini, M. Cavallini, W. J. Feast, A. F. M. Kilbinger, R. Lazzaroni, E. W. Meijer, A. P. H. J. Schenning, *J. Mater. Chem.* **2004**, *14*, 1959. g) M. Melucci, G. Barbarella, M. Zambianchi, M. Benzi, F. Biscarini, M. Cavallini, A. Bongini, S. Fabbroni, M. Mazzeo, M. Anni, G. Gigli, *Macromolecules.* **2004**, *37*, 5692.
[4] a) A. Marrocchi, M. Seri, C. Kim, A. Facchetti, A. Taticchi, T. J. Marks, *Chem. Mater.* **2009**, *21*, 2592. b) P. Sonar, S. P. Singh, S. Sudhakar, A. Dodabalapur, A. Sellinger, *Chem. Mater.* **2008**, *20*, 3184. c) M. Melucci, L. Favaretto, C. Bettini, M. Gazzano, N. Camaioni, P. Maccagnani, P. Ostoja, M. Monari, G. Barbarella, *Chem. Eur. J.* **2007**, *13*, 10046. d) M. Zhang, H. N. Tsao, W. Pisula, A. K. Mishra, K. Müllen, *J. Am. Chem. Soc.* **2007**, *129*, 3472. e) J. Peet, J. Y. Kim, N. E. Coates, W. L. Ma, D. Moses, A. J. Heeger, G. C. Bazan, *Nat. Mater.* **2007**, *6*, 497. f) Y. S. Park, D. Kim, L. Hoosung, B. Moon, *Org. Lett.* **2006**, *8*, 4702. g) D. Mühlbacher, M. Scharber, M. Morana, Z. Zhu, D. Waller, R. Gaudiana, C. Brabec, *Adv. Mater.* **2006**, *18*, 2884. h) M. Jayakannan, P. A. Van, Hal, R. A. J. Janssen, *J. Polym. Sci. Part A: Polym. Chem.* **2001**, *40*, 251.
[5] a) G. Derue, D. A. Serban, Ph. Leclère, S. Melinte, P. Damman, R. Lazzaroni, *Org. Electron.* **2008**, *9*, 821. b) P. Leclère, M. Surin, P. Brocorens, M. Cavallini, F. Biscarini, R. Lazzaroni, *Mater. Sci. Eng. Rep.* **2006**, *55*, 1. c) J.-H. Kim, M. Yoneya, H. Yokoyama, *Nature* **2002**, *420*, 159. d) G. Derue, S. Coppée, S. Gabriele, M. Surin, V. Geskin, F. Monteverde, P. Leclère, R. Lazzaroni, P. Damman, *J. Am. Chem. Soc.* **2005**, *127*, 8018.
[6] E. Kim, Y. Xia, G. M. Whitesides, *Nature* **1995**, *376*, 581.
[7] a) C. Van Pham, A. Burkhardt, R. Shabana, D. D. Cunningham, H. B. Mark, H. Zimmer, *Phosphorus, Sulfur Silicon Relat. Elem.* **1989**, *46*, 153. b) K. Meerholz, J. Heinze, *Electrochim. Acta* **1996**, *41*, 1839.
[8] a) H. A. M. van Mullekom, J. A. J. M. Venkemans, E. W. Meijer, *Chem. Eur. J.* **1998**, *4*, 1235. b) M. Karikomi, C. Kitamura, S. Tanaka, Y. Yamashita, *J. Am. Chem. Soc.* **1995**, *117*, 6791.
[9] G. Barbarella, L. Favaretto, G. Sotgiu, M. Zambianchi, A. Bongini, C. Arbizzani, M. Mastragostino, M. Anni, G. Gigli, R. Cingolani, *J. Am. Chem. Soc.* **2000**, *122*, 11971.
[10] a) *Handbook of Thiophene-Based Materials: Applications in Organic Electronics, Photonics* (Eds: D. Perepitchka, I. Perepitchka), Wiley, New York **2009**. b) G. Barbarella, M. Melucci, *Thiophene-S,S-dioxides as a Class of Electron-Deficient Materials for Electronics and Photonics*, Wiley, New York **2009**. c) G. Barbarella, L. Favaretto, G. Sotgiu, L. Antolini, G. Gigli, R. Cingolani, A. Bongini, *Chem. Mater.* **2001**, *13*, 4112.
[11] a) F. Garnier, G. Horowitz, D. Fichou, *Synth. Met.* **1989**, *28*, 705. b) A. Yassar, G. Horowitz, P. Valat, V. Wintgens, M. Hmyene, F. Deloffre, P. Srivastava, P. Lang, F. Garnier, *J. Phys. Chem.* **1995**, *99*, 9155. c) X. Zhang, J. P. Johnson, J. W. Kampf, A. J. Matzger, *Chem. Mater.* **2006**, *18*, 3470.
[12] A. R. Murphy, P. C. Chang, P. VanDyke, J. Liu, J. M. J. Fréchet, V. Subramanian, D. M. DeLongchamp, S. Sambasivan, D. A. Fischer, E. K. Lin, *Chem. Mater.* **2005**, *17*, 6033.
[13] G. Barbarella, L. Favaretto, G. Sotgiu, M. Zambianchi, C. Arbizzani, A. Bongini, *Chem. Mater.* **1999**, *11*, 2533.
[14] The solubility in CH_2Cl_2 0.1 mol L^{-1} $(C_4H_9)_4NClO_4$ of TTTBTTT and TTBTBTT was below 1.5 mmol L^{-1}, consequently CVs were recorded in saturated solutions and their signal resulted lower than that of the shorter co-oligomers; on the contrary, TyTyTBTTyTy showed much greater solubility.
[15] S. Trasatti, *Pure Appl. Chem.* **1986**, *58*, 955.
[16] G. Barbarella, L. Favaretto, M. Zambianchi, O. Pudova, C. Arbizzani, A. Bongini, M. Mastragostino, *Adv. Mater.* **1998**, *10*, 551.
[17] a) M. Melucci, Pierre. Frére, M. Allain, E. Levillain, G. Barbarella, J. Roncali, *Tetrahedron* **2007**, *63*, 9774. c) M. Melucci, L. Favaretto, G. Barbarella, A. Zanelli, N. Camaioni, M. Mazzeo, G. Gigli, *Tetrahedron* **2007**, *63*, 11386.
[18] a) C. C. Cedeno, J. Seekamp, A. P. Kam, T. Hoffmann, S. Zankovych, C. M. Sotomayor Torres, C. Menozzi, M. Cavallini, M. Murgia, G. Ruani, F. Biscarini, M. Behl, R. Zentel, J. Ahopelto, *Microelectron. Eng.* **2002**, *61–62*, 25. b) M. Cavallini, I. Bergenti, S. Milita, G. Ruani, I. Salitros, Z.-R. Qu, R. Chandrasekar, M. Ruben, *Angew. Chem. Int. Ed.* **2008**, *47*, 8596.
[19] a) M. Cavallini, C. Albonetti, F. Biscarini, *Adv. Mater.* **2009**, *21*, 1043. b) D. A. Serban, P. Greco, S. Melinte, A. Vlad, C. A. Dutu, S. Zacchini, M. C. Iapalucci, F. Biscarini, M. Cavallini, *Small* **2009**, *5*, 1117. c) M. Cavallini, *J. Mater. Chem.* **2009**, *19*, 6085. d) M. Cavallini, M. Facchini, C. Albonetti, F. Biscarini, *Phys. Chem. Chem. Phys.* **2008**, *10*, 784.
[20] J. Gratzner, J. Kuta, *Pure Appl. Chem.* **1984**, *56*, 461.
[21] *HyperChem 7.52*, Hypercube, Inc, Waterloo, Ontario, Canada.
[22] P. Damman, M. G. Zolotukhin, D. Villers, V. M. Geskin, R. Lazzaroni, *Macromolecules* **2002**, *35*, 2.

© 2010 WILEY-VCH Verlag GmbH & Co. KGaA, Weinheim